Monitoring Duration and Extent of Storm-Surge and Flooding in Western Coastal Louisiana Marshes With Envisat ASAR Data

Elijah Ramsey III, Zhong Lu, Yukihiro Suzuoki, Amina Rangoonwala, and Dirk Werle, *Member, IEEE*

***Abstract*—Inundation maps of coastal marshes in western Louisiana were created with multitemporal Envisat Advanced Synthetic Aperture (ASAR) scenes collected before and during the three months after Hurricane Rita landfall in September 2005. Corroborated by inland water-levels, 7 days after landfall, 48% of coastal estuarine and palustrine marshes remained inundated by storm-surge waters. Forty-five days after landfall, storm-surge inundated 20% of those marshes. The end of the storm-surge flooding was marked by an abrupt decrease in water levels following the passage of a storm front and persistent offshore winds. A complementary dramatic decrease in flood extent was confirmed by an ASAR-derived inundation map. In nonimpounded marshes at elevations $<$ 80 cm, storm-surge waters rapidly receded while slower recession was dominantly associated with impounded marshes at elevations $>$ 80 cm during the first month after Rita landfall. After this initial period, drainage from marshes—especially impounded marshes—was hastened by the onset of offshore winds. Following the abrupt drops in inland water levels and flood extent, rainfall events coinciding with increased water levels were recorded as inundation re-expansion. This postsurge flooding decreased until only isolated impounded and palustrine marshes remained inundated. Changing flood extents were correlated to inland water levels and largely occurred within the same marsh regions. Trends related to incremental threshold increases used in the ASAR change-detection analyses seemed related to the preceding hydraulic and hydrologic events, and VV and HH threshold differences supported their relationship to the overall wetland hydraulic condition.**

***Index Terms*—Coastal marshes, flooding, hurricanes, radar, storm surge, topography.**

I. Introduction

WETLANDS are diverse arrays of biophysical systems that exhibit large variations in areal extent, temporal duration, and spatial complexity. Coastal wetlands are linked to the productivity of the ocean and provide critical nursery areas for multitudes of coastal and oceanic life.

Manuscript received November 06, 2009; revised March 08, 2010; accepted November 03, 2010.

E. Ramsey III is with the U.S. Geological Survey, National Wetlands Research Center, Lafayette, LA 70506 USA (e-mail: elijah_ramsey@usgs.gov).

Z. Lu is with the U.S. Geological Survey, Earth Resources Observation and Science Center and Cascades Volcano Observatory, Vancouver, WA 70506 USA.

Y. Suzuoki is with ASci Corporation, Inc., Lafayette, LA 70506 USA.

A. Rangoonwala is with IAP Worldwide Services, Inc., Lafayette, LA 70506 USA.

D. Werle is with AERDE Environmental Research, Halifax, Nova Scotia, Canada B3J 2X1.

Digital Object Identifier 10.1109/JSTARS.2010.2096201

The coastal zone of Louisiana located in the central-northern Gulf of Mexico (GOM) accounts for about 40% of the coastal tidal wetland in the continental United States [1]. The zone is depicted by a gradual increase of elevation that starts at sea level at the coast and reaches 1 m to 1.5 m at the southern extent of upland prairie and forests (Fig. 1). In addition to flood events [2], [3], the seasonal and interannual marsh phenology [4] and the ephemeral nature of many small water bodies [2] in these marshes produce a highly dynamic landscape. These rapid changes must be accounted for in order to precisely identify the threshold duration of saturation required for wetland viability [5]. Our paper provides information on flood extent and distribution during a singular episodic storm event, and while approach and results do not allow immediate inference on health or trend of the marsh system, there is evidence that such storm events may cause severe stress on marsh vegetation in the region [3]. Produced systematically, maps portraying wetland vegetation condition and spatially distributed inundation could provide crucial information for linking wetland health and flood frequency and duration [6]–[9].

Passive optical remote sensing can adequately address many coastal resource management issues [10]–[13]; however, optical systems are critically limited by their dependence on sunlight and favorable weather conditions when time-constrained collections are needed [5]–[7], [9], [12], [14], [15]. Even when reliance on time-constrained collections is minimized, the restricted penetration of visible and near-infrared radiation into full cover canopies limits detection of subcanopy flooding with optical systems [6], [16], [17].

Conventional contour mapping of point measurements of water level is hampered by the high spatial variability of flood occurrences, difficulties in timing field data collections with highly dynamic flood events, and inherent problems in predicting marsh flood stage from off-site gauges [8], [18]. Hydraulic flow models can be used to predict inundation patterns [12], alleviating many difficulties inherent in conventional contouring. Lack of the necessary spatial density of stage measurements and the prevalent disconnect between marsh and off-site measured flows, however, diminish the capability to provide hydraulic model calibration and validation [9], [19]. To help overcome these difficulties in monitoring and simulating the spatially distributed and rapidly changing nature of coastal inundation, remote sensing synthetic aperture radar (SAR) systems are used.

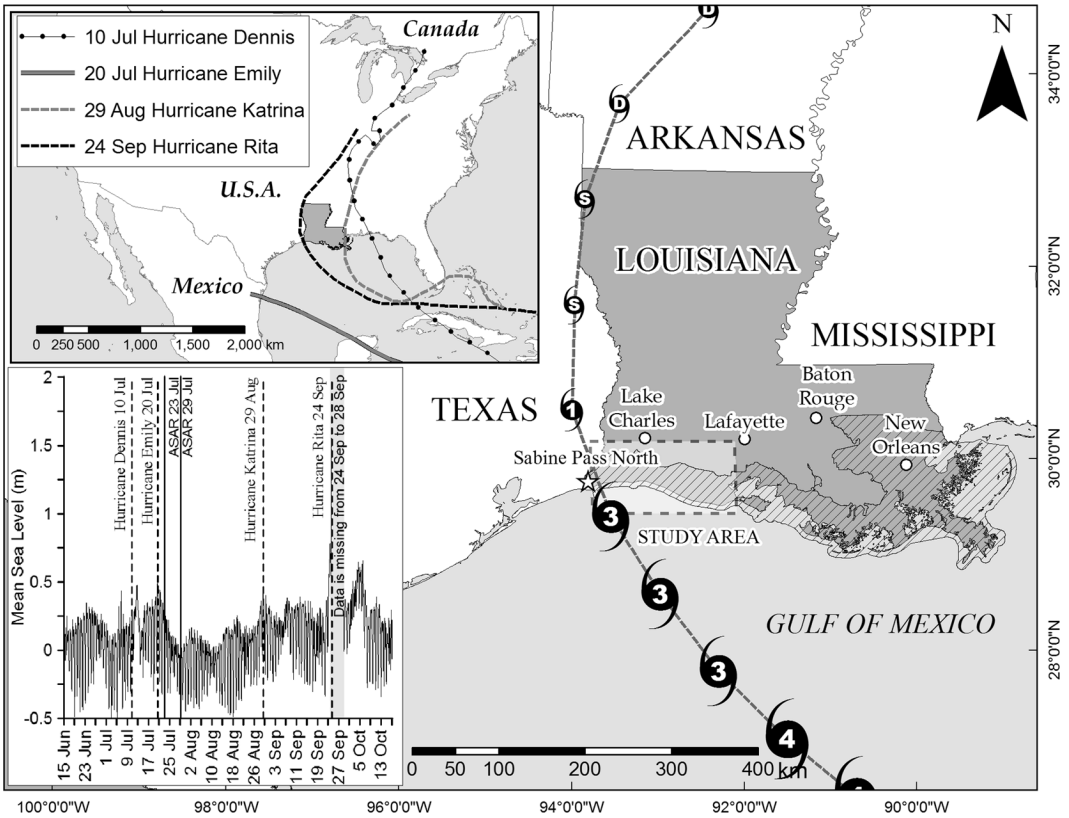

Fig. 1. Study area and Hurricane Rita. The subset image shows paths of other major hurricanes in the Gulf of Mexico during the study period. Track numbers denote hurricane category at each location. A partially opaque box indicates the study region and hatched area represents the Louisiana Coastal Zone. The hydrographic data show the storm-surge hydrograph at Sabine Pass North from 15 July to 15 October 2005 (Gauge was not functioning at the surge peak) [38]. The coastal hydrologic station captured the elevated water levels related to each hurricane (http://tidesandcurrents.noaa.gov/gmap3/). (See the subset image for each hurricane path.).

Microwave remote sensing systems offer a viable alternative data source when timely and consistent collections are dominant concerns [19]–[22]. SAR sensors operating at centimeter wavelengths can collect information day and night and in most weather conditions and provide increased canopy penetration [6], [7], [14], [16], [23]. Satellite-based radar sensors, such as the C-band advanced SAR (ASAR) aboard the European Space Agency's (ESA) Envisat, the C-band SAR aboard the Canadian Space Agency's Radarsat sensors, the X-band SAR aboard the German TerraSAR-X, and the Phased Array type L-band SAR (PALSAR) aboard the Japanese Advanced Land Observing Satellite (ALOS), have proven to be valuable tools for surveying land and water surfaces during weather-related emergencies [24].

Although increased canopy transmittance of longer wavelengths implies superior subcanopy inundation mapping with SAR systems operating at L-band [6], [14], [20], the C-band ASAR flood mapping has performed well in Louisiana marshes as it has in other marshes occupying the northern GOM coasts [2], [3], [8], [20] and elsewhere [7]. Using SIR-C SAR C-band and L-band HH and VV data, Pope *et al.* [25] demonstrated that herbaceous (marsh) subsurface flooding can be exhibited as an increase or decrease in SAR backscatter. In effect, the nature of the change and the ability to differentiate between flooded and nonflooded marshes depend on the marsh type, height, density, stem orientation and size, soil moisture, inundation depth and history, as well as the SAR sensor parameters [20], [25], [26].

In coastal marshes occupying the northern and eastern GOM, the interrelation between these biophysical variables and incident SAR C-band signals dominantly produce a backscatter decrease in flooded versus nonflooded marshes. For example, in the northeastern GOM, field validated [8] and modeled [27] ERS SAR C-band VV backscatter were lower from flooded than from nonflooded marsh. In a variety of southeastern GOM marshes, Kasischke *et al.* [20] substantiated the progressive decrease in ERS C-band VV backscatter with increasing flood level and a positive relationship between soil moisture and SAR backscatter. In the north-central GOM, Kiage *et al.* [2] documented decreased Radarsat SAR C-band HH backscatter from hurricane surge-flooded saline, brackish, and fresh coastal marshes compared to presurge scattering conditions and SAR signatures. Even the TerraSAR X-band system was used to successfully estimate water-level changes in south Florida marshes [28]. In addition, any polarization influence on the flood mapping effectiveness (e.g., [25], [26]) was expected to favor the copolarization (VV and HH) ASAR data applied in this study as compared to cross-polarization (HV and VH) SAR data (e.g., [12]). Trends observed and modeled in northern GOM fresh to saline coastal marshes have consistently docu-

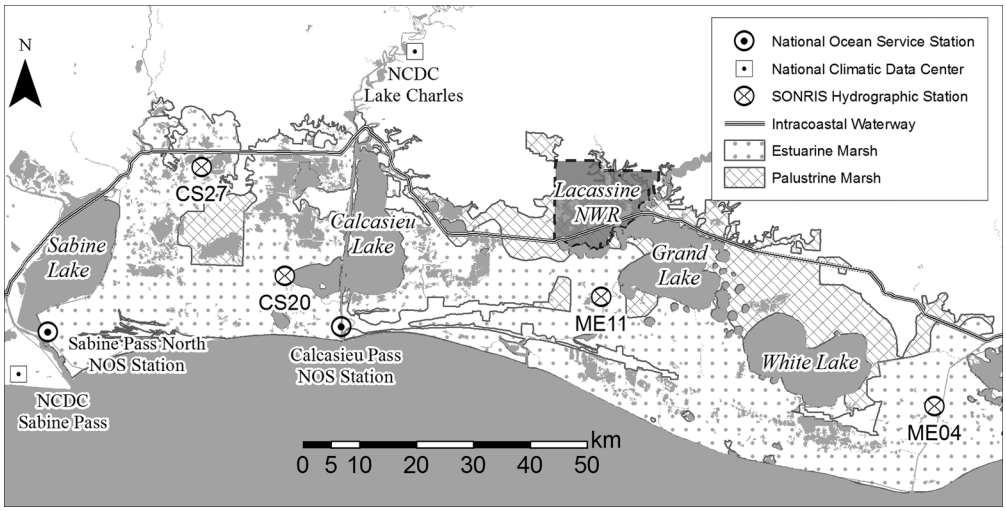

Fig. 2. Hydrographic and weather station locations [34], [38], [39]. The white stippled area designates estuarine marsh and the hatched lines palustrine marsh within the Louisiana coastal zone [36]. The triple line shows the Intracoastal Waterway that runs through the entire southern Louisiana coast. The dark opaque box with dotted lines shows the location of Lacassine National Wildlife Refuge.

mented decreased C-band HH and VV SAR backscatter from flooded versus nonflooded marshes.

The goal of this study is to demonstrate the ability of SAR satellite imagery to monitor the distribution and prolonged occurrence of storm-related flooding in an inland coastal wetland. Our demonstration is based on monitoring the extent and duration of storm-surge flooding of coastal Louisiana related to category 3 Hurricane Rita that made landfall on 07:40 AM UTC 24 September 2005 [29] (Fig. 1). The 3.8 m storm surge flooded the entire coastal region and pushed elevated salinity waters north beyond the ICW (Intracoastal Waterway) [1] (Fig. 2). Based on storm-surge flooding of southwest Louisiana, the objectives as part of our study goal were as follows:

1) to derive postsurge inundation distributions from available SAR scenes;
2) to combine the inundation distributions into a history of storm-surge recession;
3) to document controls that modified the postsurge recession history;
4) to spatially associate the postsurge inundation history with the occurrences of palustrine and estuarine marshes.

We provide this information based upon routine measurements that are cost-effective and easily implemented into operational resource management and verified and calibrated with current operational ground-based measurements [30].

II. Study Area

The study area for Hurricane Rita impact included coastal wetlands occurring in the central to western Louisiana coastal zone located in the north-central Gulf of Mexico (Fig. 1). Stretching along the gulf shore is a nearly continuous band of highly permeable sand and shell (cheniers) protecting extensive back barrier marshes that extend inland 6 km to 24 km, commonly at less than 1.5 m above mean sea level with slopes of less than 0.2 m per km [31] (Fig. 2).

The central-western Louisiana coastal marsh zone is dominantly underlain by frequently saturated soils. In this zone, subsurface faulting can produce surface subsidence that results in marsh submergence and fragmentation, and ultimately the formation of permanent water bodies [2], [32]. In addition, hurricanes scour the marsh creating small water bodies [1], and push elevated salinity waters into fresher marshes causing salt burn [1], [3]. Aggravating these detrimental impacts are channels and levies, as well as impoundments constructed to provide transport conduits and waterfowl sanctuaries that impede overland flow. These impediments can lengthen the marsh exposure to elevated salinity water and, in the case of intense rainfall accompanying storm events, prolong inundation and promote water logging that can advance marsh alteration and deterioration. The combination of low topographic relief, poorly drained soils, tectonic activity, and flow impedance creates a spatially complex hydrological landscape.

III. Methods

A. Image Data Collection, Calibration, and Registration

A total of eight Envisat ASAR scenes, including seven Wide Swath Mode scenes at a nominal spatial resolution of 150 m and one Image Mode scene at a nominal spatial resolution of 30 m were used in the present study (Fig. 3). The eight scenes included all available and pertinent Wide Swath and Image Mode data collections that took place within the previous summer months and three months after the landfall of Hurricane Rita. Incidence angles ranged from 16° in the near-range to 36° in the far-range of the imaged swath (Table I, Fig. 3). The 1 October 2005 Image Mode ASAR scene did not cover the entire east to west extent of the study area. To allow scene-to-scene comparability, the four vertical transmit and receive (VV) and four horizontal transmit and receive (HH) polarized ASAR scenes were transformed to sigma naught backscattering coefficient (σ_o) estimates using Next ESA SAR Toolbox (NEST) software and calibration coefficients provided by the ESA [33].

TABLE I
ENVISAT ASAR PARAMETERS AND ACQUISITION DATES

Sensor	Polarization	Date	Incident Range covering Study Area	Track
ASAR/WSM	HH	23 July 2005	16.3 - 26.5	162
ASAR/WSM	VV	29 July 2005	34.2 - 42.6	248
ASAR/IMP	VV	1 October 2005	18.6 - 26.1	162
ASAR/WSM	VV	20 October 2005	20.7 - 31.5	434
ASAR/WSM	VV	8 November 2005	25.5 - 35.9	205
ASAR/WSM	HH	24 November 2005	20.3 - 31.3	434
ASAR/WSM	HH	13 December 2005	25.2 - 35.9	205
ASAR/WSM	HH	29 December 2005	20.3 - 31.7	434

IMP: Image Mode Precision Image, WSM: Wide Swath Mode Image

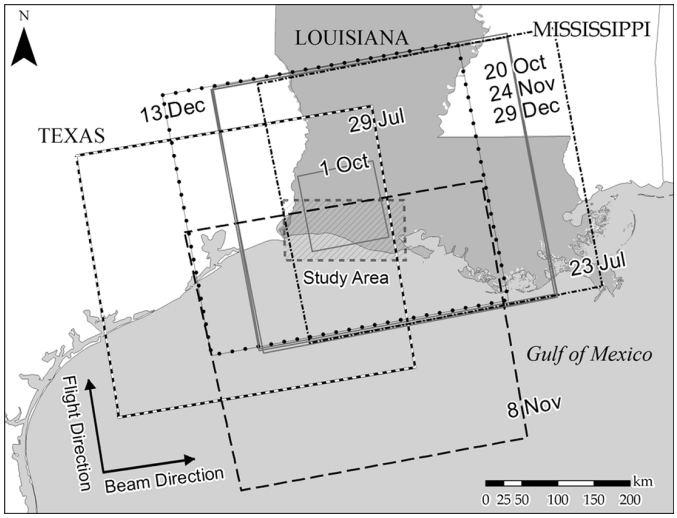

Fig. 3. Envisat ASAR Louisiana Coastal Coverage. All images are in ascending mode and incidence angles increase from left to right. (See Table I for track information.)

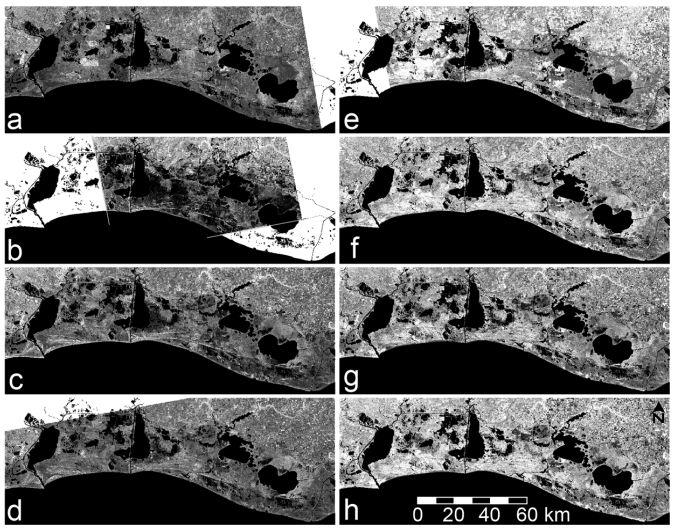

Fig. 4. The calibrated and georeferenced ASAR scenes with VV polarization collected on (a) 29 July 2005, (b) 1 October, (c) 20 October, and (d) 8 November, and ASAR scenes with HH Polarization collected on (e) 23 July 2005, (f) 24 November, (g) 13 December, and (h) 29 December. Grey levels are comparable in all ASAR scenes; brighter denotes higher backscatter. White areas depict the lack of ASAR coverage. Areas lacking coverage were removed from all scenes before storm-surge analyses.

All satellite data were registered to a Landsat Thematic Mapper (TM) Lambert Conformal Conic (LCC) base image. The LCC projection eliminated problems of multiple Universal Transverse Mercator (UTM) zones. The LCC projection used the WGS84 geoid and the projection parameters defined by the Louisiana State Plane Coordinate System. Areal distortion for the studied area was measured as $<0.01\%$.

The base TM LCC projection accuracy was assessed by comparison to U.S. Geological Survey Digital Ortho Quarter Quads (DOQQs). Rectification errors of the LCC base TM to the DOQQs were generally less than 0.5 pixels. TM and ASAR registration errors ranged between 0.2 and 0.5 pixels. All registered ASAR scenes were created at a 75 m spatial resolution to promote compatibility with other satellite data sources. The eight calibrated and georeferenced ASAR scenes are depicted for the study area in Fig. 4(a)–(h).

B. Inland Surge Hydrographs

Water-level data for calibrating and validating the inundation maps were obtained from the Strategic Online Natural Resources Information System (SONRIS) from the Louisiana Department of Natural Resources [34]. For most sites, the hydrographic records for the period before, during, and after Hurricane Rita turned out to be incomplete. Avoiding incomplete hydrograph records, we gathered four water-level hydrographs from the western coastal region (shown in Fig. 2). Water levels were corrected for biofouling, instrumental drift, and erroneous data but could not be adjusted to the local vertical datum. The lack of absolute vertical reference limited the direct comparability of the hydrographic data from site to site.

In addition, inspection of DOQQs found that the placement of the four hydrograph stations did not allow direct comparison between the observed water levels and surface inundation calculated with ASAR data. Sites ME04, CS27, and ME11 were located in water channels that exhibit different flow dynamics than those of the marsh platform and were separated from the marsh platform by varying distances and partial obstructions, such as levies. In addition, all three of the above hydrographic sites were in a mixed marsh and forest stand landscape, and site CS20 was located in degrading marsh containing a high proportion of open water. The decoupling of measured water levels from those occurring within the marsh platform and the contamination of the ASAR pixel by mixed nonmarsh land covers prevented the direct determination of marsh flooding from the

available hydrograph data. Even though unsuitable for absolute validation, the occurrence or absence of elevated water levels at the hydrographic stations provided an indication of flooding in the surrounding marshes, and thus, an additional measure of flood detection performance.

1) Permanent Water Body Delineation: In order to minimize confusion between wind-roughened water surfaces, flooded marsh, and nonflooded marsh, permanent water bodies were defined within the study area. The location and extent of permanent inland coastal waters were obtained from the Louisiana Oil Spill Coordinator's Office (LOSCO) [35] and updated with five TM images collected from 2004 to 2005 before Hurricane Rita (27 April 2004, 17 August 2004, 5 November 2004, 16 May 2005, 21 September 2005). These TM images were registered to the same LCC projected TM-base image used for the ASAR scene registrations. LOSCO permanent water polygon coverage was superimposed on the suite of TM images, and differences between the vector coverage and the TM images were determined. Differences were minor. Of the LOSCO permanent water coverage, 70 km^2 exhibited the spatial and temporal consistency of marsh throughout the 2004 and pre-hurricane 2005 suite of TM images. This area was classified as semipermanent water and removed from the original LOSCO permanent water coverage. The remaining permanent water coverage was excluded in the ASAR change-detection products.

C. Storm Surge Residual Flooding

The calibrated ASAR scenes were entered into a change-detection algorithm that incorporated an internal SAR speckle filter to dampen noise while preserving edges and shape. The 5 by 5 pixel Kuan filter best preserved edges and retained inundation spatial continuity. Each post-hurricane ASAR scene was paired with the same HH or VV pre-hurricane scene in order to eliminate change artifacts associated with SAR polarization differences. A logarithmic ratio of the before and after scenes resulting in a positive decibel difference indicated lower post-ASAR versus pre-ASAR intensities, and in these marshes, possible inundation. In addition, to help limit noise and better discriminate flooded from nonflooded marsh, a minimum change detection threshold was applied.

The ASAR image processing procedure to determine the minimum change detection threshold is not an automated one, and it relies on operator intervention and judgment to determine the threshold. In principle, this required consideration of radar parameters for imaging flooded and nonflooded terrains as well as background knowledge of flood condition and behaviour within a specific geographic setting; both aspects are brought to bear in an informed trial-and-error procedure to determine the extent and configuration of flooded versus non-flooded boundary lines. In this specific case, we also checked threshold flood extents for consistency by comparing results with the original ASAR data, by comparing them with the closest date of TM and inland water levels, and categorized the terrain over a wide area by either over- or under-"saturating" it in such a way that known high ground was definitively excluded from contiguous 'flooded' pixels and known low-lying flood-prone areas were included. Added to this more visual threshold selection method, we tested a more automated method of threshold section.

1) Storm-Related Residual Inundation Duration: Once the series of inundation maps were produced, the storm-surge inundation duration at each location within the 1 October coverage was calculated. The spatial distribution and extents of each of the separate inundations were overlain and their intersections were used to define areas of constant flooding from 1 October. Each intersection depicted the duration between ASAR scene collection times. For instance, 6 days and 21 hrs had elapsed between the storm landfall on 24 September and the first ASAR image collection (1 October). There was a difference of 19 days between the first and second (20 October) ASAR data-acquisition date, 19 days between the second and third (8 November), and 16 days between the third and fourth (24 November) date. This ASAR data-acquisition schedule established a scenario of four surge-associated flood durations that varied in length by approximately 7 days, 26 days, 45 days and 61 days, respectively.

D. Wetland Class and Flood Duration

The spatial distribution of marsh classes throughout the Louisiana coastal zone was obtained from the 2007 Louisiana Coastal Marsh Vegetation Type Map [36]. Herbaceous wetland classes included palustrine marsh, intermediate marsh, brackish marsh, and saline marsh. The intermediate, brackish, and saline marshes were combined into the estuarine marsh class to generalize the comparisons and to better align with national wetland classification systems [10] (Fig. 2). The ASAR Image Mode scene included 1,654 km^2 of estuarine and 797 km^2 of palustrine marshes and ASAR Wide Swath Mode scenes included 3,212 km^2 of estuarine and 979 km^2 of palustrine marshes. The calculated maps of flood duration were superimposed on the coastal wetland classification to establish categories of flood duration and marsh type.

E. Topography and Flood Duration

A topographic LIDAR survey performed in 2002 was used to calculate the covariance between inundation extent and duration and elevation [37]. The digital elevation model (DEM) coverage was created at a posting interval of 5 m, and the DEMs used in this study exhibited elevation accuracies better than 15 cm. The DEM coverage aggregated at 20- cm intervals and superimposed on the derived inundation maps produced associations of inundation and coastal topography.

IV. Results

A. Change-Detection Base Scenes and Thresholds

1) Prehurricane ASAR Scenes: Sea level was elevated from mid-August onward as a result of the approaches and landfalls of Hurricanes Katrina and Rita. Previous to this run-up period, two ASAR scenes were available as candidate pre-hurricane scenes for the change-detection analyses. An overlay of the two summer season ASAR scene-collection times onto a coastal hydrograph obtained from the National Ocean Service showed that the 23 July ASAR HH scene was collected near the end of an abnormally high sea level (Fig. 1, [38]). The higher sea level

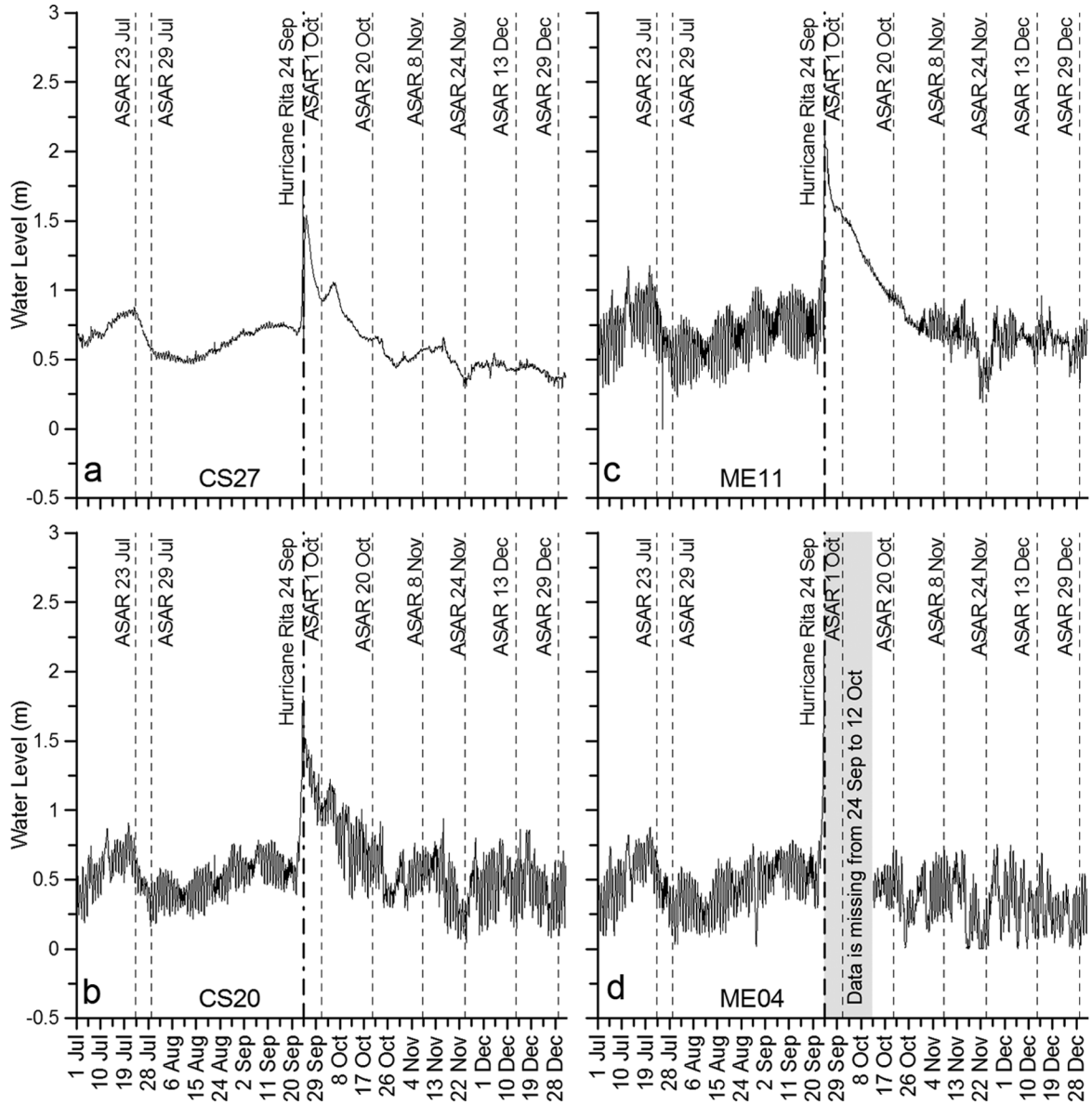

Fig. 5. Inland storm-surge hydrographs. (a) CS27, (b) CS20, (c) ME11, and (d) ME04 hydrographs were recorded relative to each instrument sensor and corrected for biofouling and instrument drift. Data were obtained from SONRIS [34]. Water levels were not comparable from station to station.

was most likely associated with the occurrences of Hurricanes Dennis and Emily in the gulf on 10 and 20 July 2005 (Fig. 1). Inland hydrographs showed an elevated water surface remained on 23 July 2005 (Fig. 5). Even though pre-hurricane scenes collected during normal sea levels were preferred, the lack of better alternate scenes and the near consistency in seasonality resulted in the use of the pre-hurricane ASAR Wide Swath Mode HH and VV scenes collected on 23 and 29 July. The reasonableness of using the non-ideal pre-hurricane ASAR HH scene was determined in the post-Hurricane Rita inundation analyses.

Although elevated water levels were not expected to be problematic in the pre-hurricane ASAR scenes, the 23 July 2005 ASAR HH scene exhibited relatively high SAR returns in the near-range of the scene (Fig. 4(e)). These elevated returns could lower change analysis performance in the extreme southwestern edge of the study area by abnormally increasing the contrast between before and after hurricane ASAR scene data. Visual interpretation of the pre- and post-hurricane HH ASAR scenes, however, did not suggest that subcanopy flooding was incorrectly mapped in the southwestern extent of the study region. Changing extents mimicked changes in inland water-level trends. In essence, even though pre-hurricane HH ASAR backscatter was elevated in the near-range of the study area, results did not indicate that inundation was spatially over-extended in the southwest region of the study area.

2) Inundation Threshold: The total area associated with positive change-detection results above each incremental increase of threshold magnitude was calculated for each post-hurricane ASAR date as compared to the original pre-hurricane ASAR scene. Inflections in the plotted trends were sought to indicate an abrupt change in the SAR response possibly related to a change from flooded to nonflooded marsh. All six curves decreased without an obvious inflection point throughout the threshold ranges evaluated (Fig. 6). Lacking an inflection point indicating

TABLE II
WATER LEVELS AT INLAND COASTAL HYDROGRAPHIC STATIONS

ASAR date	Water Level (m)			
	CS20	ME04	CS27	ME11
23 July 2005	0.506	0.488	0.838	0.671
29 July 2005	0.463	0.384	0.576	0.686
1 October 2005	1.042	no data	0.924	1.524
20 October 2005	0.826	0.704	0.646	0.963
8 November 2005	0.713	0.640	0.567	0.890
24 November 2005	0.347	0.366	0.372	0.518
13 December 2005	0.512	0.384	0.433	0.579
29 December 2005	0.445	0.268	0.375	0.506

Station locations are shown on Fig. 2. Sites CS27 and ME04 were not included in the 1 October ASAR scene coverage.

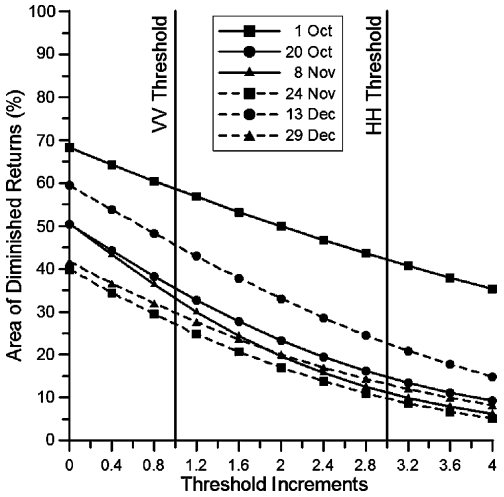

Fig. 6. Positive change-detection thresholds trends (the before backscatter intensity is higher than the after hurricane intensity). Each trend line is normalized by the ASAR scene coverage. Inundation distributions on Fig. 7 are related to areas above the VV (at 1) and HH (at 3) thresholds.

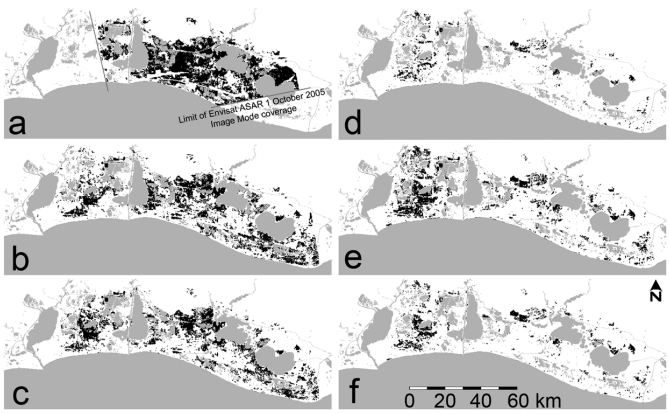

Fig. 7. Distribution maps of post-hurricane residual flood. ASAR flood detection denoted as black areas from change detection based on (a) 29 July to 1 October, (b) 29 July to 20 October, (c) 29 July to 8 November, (d) 23 July to 24 November, (e) 23 July to 13 December, and (f) 23 July to 29 December. All permanent water bodies created from LOSCO [35], and 2004 and 2005 pre-hurricane TM images were subtracted from results to avoid confusion with flooded marsh. Table III includes the estuarine and palustrine inundation associated with (a) to (f).

an abrupt change, choice of threshold values was guided by inland water levels and visual interpretation. Threshold magnitudes of 1.0 dB (VV) and 3.0 dB (HH) were found to retain trends observed in the inland hydrographic measurements and visual interpretation of inland inundation extents.

Even though not providing abrupt delimitation, the threshold curves provided an overall snapshot of the current hydrologic status of the marsh (Fig. 6). Parameterization of the threshold and area relationships produced second order polynomials that explained >99% of each trends' variance. Each polynomial equation provided an intercept (INT) indicating the percentage of positive changes and a linear versus curvilinear trend indicator (LI) as the first and second order coefficient ratio. The parameterized threshold trends showed that the 1 October relationship had the highest total magnitudes (INT = 0.68) and most linear response (LI = 11.01) followed by 13 December (INT = 0.60, LI = 7.40). Both dates followed inundation events; storm surge in the first case and rainfall events in the latter. Outside of these two distinctive trends, intercepts are reduced in parallel with reductions in water level. The 20 October and 8 November VV trends had an INT of 0.51 and LIs of 5.11 and 4.52, respectively. The 24 November and 29 December HH trends had INTs of 0.40 and 0.42 and LIs of 5.14 and 5.41, respectively.

B. Storm-Surge Hydrographs

Four inland hydrographs confirmed the occurrence of surge flooding throughout the western coastal region (Figs. 2 and 5). In comparison to pre-hurricane 23 and 29 July water levels, all working hydrographs exhibited elevated water levels on 1 October and although abated, elevated water levels persisted through 20 October at all hydrograph stations (Table II). Water-level records indicated some shallower flooding persisted through 8 November. Just prior to the 24 November collection, all four hydrographs exhibited an abrupt decrease in water levels and, shortly thereafter, a rapid increase preceded the 13 December ASAR collection. Subsequently, surface water levels decreased through 29 December.

1) Inundation Extent and Water Level: The distribution maps of post-hurricane residual floods prepared from the six ASAR dates were in agreement with the temporal patterns of water levels recorded at the operating hydrographic stations (Figs. 5(a)–(d) and 7(a)–(f)). Total flooded area observed at each post-hurricane ASAR date was compared to the recorded inland water levels (Table II). In each of the comparisons, >95% of the variability in flood area was explained by water level (Fig. 8).

TABLE III
INUNDATION EXTENT RELATED TO MARSH TYPE

Change-Detection Images	Inundation, Percentage of Area		
	All Marsh	Estuarine Marsh	Palustrine Marsh
29 Jul to 1 Oct	48.0%	44.7%	54.8%
29 Jul to 20 Oct	23.4%	21.8%	28.5%
29 Jul to 8 Nov	20.2%	18.1%	27.1%
23 Jul to 24 Nov	4.8%	3.7%	8.4%
23 Jul to 13 Dec	14.1%	12.6%	19.3%
23 Jul to 29 Dec	7.3%	5.1%	14.6%

Change detection percentages are related to ASAR scene coverages indicated on Fig. 7.

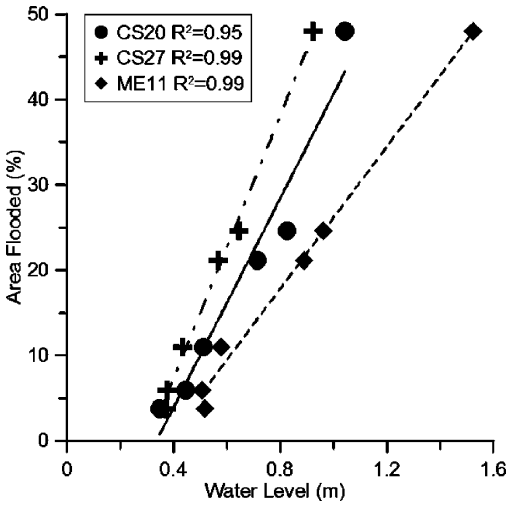

Fig. 8. Flooded area percent observed on the six ASAR post-hurricane dates and inland water level measured at hydrograph stations (locations shown on Fig. 2). The lines represent linear regression predictions. ME04 was not used because of missing data.

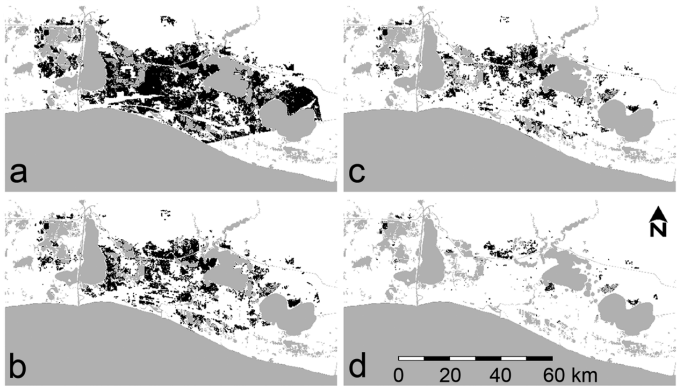

Fig. 9. Hurricane-surge related inland flooding durations. The three separate duration maps were created from the intersection of the flood extent maps displayed in Fig. 7(a)–(d). Surge flood maps correspond to durations of at least (a) 7 days, (b) 26 days, (c) 45 days, and (d) 61 days. As in Fig. 7, all permanent water bodies are excluded. Table IV includes the estuarine and palustrine storm-surge flooding associated with (a) to (d).

C. Storm-Surge Flood Maps and Marsh Inundation

The residual inundations were generally spatially coincident from 1 October to 29 December, and the post-hurricane residual inundation extent generally decreased with time past hurricane landfall (Fig. 7(a)–(d)). Although some inconsistencies occurred at scattered pixels, surge inundation impacting 48% of the marshes 7 days after landfall had progressively receded to 20% of the coastal marshes 45 days after landfall (Table III). On 24 November, the progressive postlandfall reduction in marsh flooding was interrupted by a sudden decline to 5% and a subsequent increase to 14% of the coastal marshes on 13 December (Table III, Fig. 7(d) and (e)). This progressive trend and dramatic drop in flood extent was documented in hydrographic measurements (Fig. 5(a)–(d)). These measurements also revealed a water level increase previous to the 13 December ASAR collection and the subsequent successive decrease that was reflected as inland inundation recession on 29 December. The last two flood inundation distributions on the 13 and 29 December did not appear directly related to the storm surge (Fig. 7(e) and (f)). These dates were not included in the surge inundation-duration calculations.

D. Storm-Surge Flood Duration

The post-hurricane storm-surge-related flood maps were restricted to the 1 October flood coverage (Fig. 9(a)–(d), Table IV). For 7, 26, and 45 days, respectively, residual hurricane storm-surge flooding continuously covered 45%, 20%, and 12% of the estuarine and 55%, 27%, and 19% of the palustrine marshes. The longest possible storm-surge duration persisted until 24 November, more than two months after landfall, and impacted 1% and 7% of the estuarine and palustrine marshes, respectively (Fig. 9(d), Table IV). The longest persistent surge-related inundation durations were almost entirely confined to inland pools located in the palustrine marshes.

The intersection-overlay technique used to calculate storm-surge durations was also used to calculate the spatial juxtaposition of each subsequent flood extent on the previous flood extent for the overlapping scene coverage. These calculations found that 90% of the 20 October extent was contained in the 1 October inundation extent. A drop to 73% alignment between 20 October and 8 November was primarily associated with expanded flooding in a contiguous marsh area in the east. The increased flooding may have been in response to persistent onshore winds and higher tides preceding the 8 November ASAR collection (Fig. 10). The flood distribution was well aligned at 82% from 8 to 24 November but decreased substantially to 33% between 24 November and 13 December. The latter nonalignment was caused by the dramatic decrease in flood extent on 24 November and re-expansion by 13 December. The 13 December inundation primarily expanded into the previous 8 November inundation extent (63% overlap). The 13 and 29 December inundation distributions were highly aligned at 88%.

TABLE IV
STORM-SURGE FLOOD DURATION RELATED TO MARSH TYPE.

Storm-Surge Duration	Flood Duration, Percentage of Area		
	All Marsh	Estuarine Marsh	Palustrine Marsh
7 days 24 Sep until 1 Oct	48.0%	44.7%	54.8%
26 days until 20 Oct	22.3%	20.2%	26.7%
45 days until 8 Nov	14.2%	11.7%	19.3%
61 days until 24 Nov	2.8%	1.0%	6.5%

Flood durations are related to the 1 October coverage shown on Fig. 9.

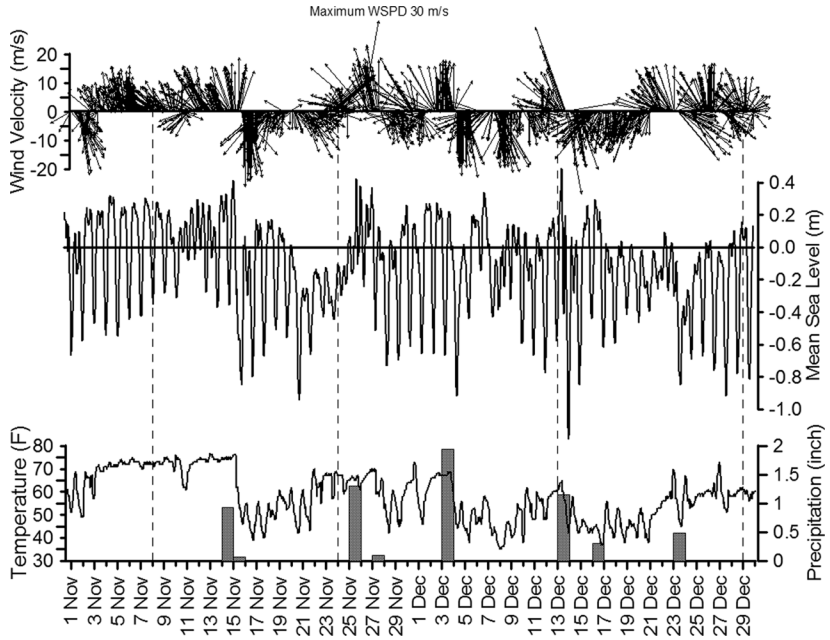

Fig. 10. Wind velocity (Sabine Pass NCDC Station) – top [39], water level (Calcasieu Pass NOS Station) – middle [38], and air temperature (Sabine Pass NCDC Station) and precipitation (bars) (Lake Charles NCDC Station) – bottom [39]. The hydrograph data was obtained from the NOAA coastal site located on Fig. 2. Dashed lines indicate 8 November and later ASAR collections.

E. Linking Inundation Duration and Topography

Restricted to flooding spatially coincident with the 1 October flooding, overlay of 20-cm elevation intervals and the 1 October through 24 November surge-related flood period documented the relationship between marsh surface elevation and inundation extent at each date (Fig. 11). Exclusion of the permanent water bodies primarily occupying the 0 cm to $<$ 20 cm elevation interval probably accounted for the relatively lower numbers in the $<$ 20 cm interval. The change in surge-related flooding between dates exhibited similar trends for elevations 0 cm to $<$80 cm and another for elevations$>$100 cm to 140 cm. The 0 cm to $<$80 cm trends indicated a rapid 53$\pm$3% decrease in storm-surge coverage from 1 to 20 October, a low decrease around 17$\pm$4% from 20 October to 8 November, and a slight rise in storm-surge recession to 24$\pm$1% from 8 to 24 November. Elevations 100 cm to $<$140 cm portrayed a moderate 30$\pm$3% decrease from 1 to 20 October, a moderately low 15$\pm$3% decrease from 20 October to 8 November, and a high decrease of 44$\pm$5% from 8 to 24 November. The inundation decrease in the transition 80 cm to $<$100 cm interval was moderately rapid initially at 38% and remained comparatively constant after that at 26$\pm$2%.

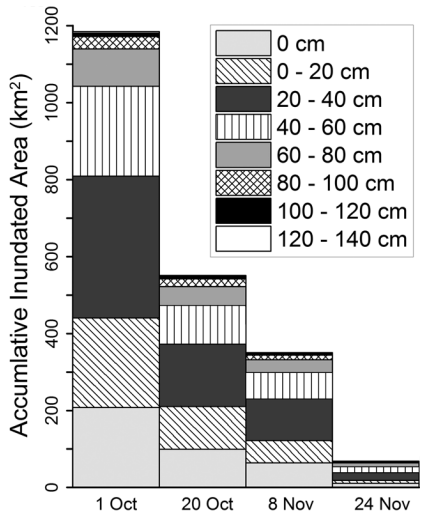

Fig. 11. The stacked-accumulative bar graphs represent the distribution of inundation by elevation aggregated at 20-cm intervals (e.g., on 1 October, 207 km^2 of the 0 cm elevation, 232 km^2 of the 0–20 cm, 368 km^2 of the 20–40 cm, 233 km^2 of the 40–60 cm, etc. elevation ranges were inundated). Permanent water bodies are excluded from the calculation. The calculation is restricted to the 1 October ASAR coverage.

V. Discussion

Flood detection by means of ASAR change-detection analysis relied on the well-documented and distinct signature of attenuated SAR returns from inundated marsh. Even though distinctive, the multiplicity of possible interactions related to changing marsh flood depth with respect to canopy height yielded complex SAR representations of the post-hurricane marshes. Pairing before and after hurricane scenes by polarization and, as much as possible, choosing pre-hurricane scenes with minimum flooding promoted post-hurricane flood-detection performance. Identifying and removing open water bodies from the inundation detection eliminated confusion between wind-roughened water surfaces and marsh [40]. Application of change-detection thresholds further refined the discrimination of flooded from nonflooded marsh.

As indicated in the threshold curves, intensity transitions from flooded and nonflooded marshes were gradual, reducing the potential for successful application of automated contouring of flooded pixels without the use of an interpreted threshold. Model simulations and field validations conducted in a variety of eastern GOM marshes may explain the difficulties in automatic determination of the flood to nonflood transition [20], [27]. Both model and field results demonstrated a decrease in C-band VV backscatter with increasing flood depth; however, both also observed increasing backscatter with increasing biomass when flooded, while conversely, decreasing SAR backscatter with increasing biomass in nonflooded marshes. Those results combined with the positive relationship between soil moisture and SAR backscatter [20] and a complex wetland landscape would coalesce competing interactions influencing the SAR backscatter within the flood to nonflood transition zone. Automated procedures would have to cope with these competing factors in order to provide consistent delineation. In conjunction with manually determined inundation thresholds, however, the threshold curves could provide a simple indicator of overall marsh hydraulic change, and help improve soil moisture monitoring, especially at low and high moisture contents underlying varying canopy densities and heights. Within these threshold trend differences, the VV and HH threshold values highly differed.

The VV and HH threshold difference could be related to the relatively lower incidence angle of the pre-hurricane HH ASAR scene and the enhanced backscatter from moist soils. In these nearly flat coastal landscapes that dominantly support marshes that exhibit an overall vertical orientation [41], increases in incidence angle would tend to increase attenuation and decrease backscatter [14]. The more vertical canopy orientation would enhance the interaction and attenuation of VV polarizations with the marsh canopy and in contrast enhance HH interaction with the marsh subcanopy [14], [42], [43]. The higher incidence angle of the pre-hurricane HH ASAR scene and the tendency for higher penetration of the HH than VV polarizations in these marshes would promote HH versus VV surface interaction. This surface interaction preference related to HH polarization may in part explain why HH tends to provide higher contrast between flooded and nonflooded marsh and higher coherence than associated with VV polarization [14], [26], [28].

The pre-hurricane HH scene was chosen to best represent nonflood periods when the underlying soil would be more likely to be unsaturated in contrast to the post-hurricane period. Although at and above soil saturation the incident SAR is reflected away from the sensor decreasing the response [14], [44], soil moisture up to saturation enhances backscatter [20], [44]. In this case, the higher canopy penetration tendency of HH versus VV and the lower incidence angle lessening canopy interaction would likely promote an overall higher pre-hurricane HH versus VV marsh response. The higher potential penetration of HH versus VV could also produce a larger number of diminished post-hurricane returns through increased specular reflection from oversaturated soils, especially when scattered pooling is often prevalent as well [8]. A combination of higher HH penetration and pre-hurricane unsaturated and post-hurricane saturated soils may have produced the substantially higher HH versus VV threshold.

Strong correlation was found between water level and flood extent and flooding and recession mostly took place within the same marsh regions. Even though these relationships existed, we found that changing rates of storm-surge recession were not strongly related to incremental changes in marsh elevation but more to broadly defined elevation ranges. For elevations < 80 cm, flood recession was mainly associated with nonimpounded marshes. These marshes exhibited a pattern of rapid recession in storm-surge flooding followed by a slower decrease and then a slight recession increase most likely related to the offshore winds. Above 80 cm, the storm-surge recession pattern was largely controlled by the drainage of impounded marshes. Impounded elevations 80 cm to <100 cm initially displayed a transition pattern of high recession followed by a fairly steady and moderate discharge. Impounded marshes at elevations from 100 cm to >140 cm had moderate drainage initially that decreased to a low drainage rate by the mid storm-surge recession period. Drainage in the final recession period augmented by offshore winds was rapid.

Surge flooding impacting 48% of the estuarine and inland palustrine marshes 7 days after landfall progressively receded to 20% of the coastal marshes 45 days after landfall. Only the sudden decline in residual flood extent on 24 November and subsequent increase on 13 December interrupted the progressive decrease in extent. Based on the flood extent and water level correspondence, we separated the inundation into two parts. First, flooding up to 24 November represented persistent storm-surge inundation. Second, the spatial expansion of inundation after 24 November to 13 December represented nonsurge related flooding. The nonsurge flooding persisted from 45 to 96 days of continuous flooding; it was mainly associated with palustrine marshes.

The cause for the sudden drop and subsequent rise in flood extent apart from the storm surge was not directly determined in this study, but these contractions and expansions in inundation extent may likely be related to the local wind field and rainfall events. After mid-November, a cold front passage associated with increased offshore winds coincided with a period of lowered water levels that persisted through the 24 November ASAR collection (Fig. 10). The change from onshore to offshore winds produced an abrupt drop in water levels that was recorded

by the inland hydrographs and by a decrease in residual storm-surge flood extent captured by sequential ASAR change-detection processing. The onset of these offshore winds was credited with pushing out elevated saline waters that had been held in the Lacassine NWR impounded fresh marsh (Fig. 2) since the storm-surge impact [45].

Around the time of the 13 December ASAR collection, wind speeds were some of the lowest recorded during the study period (Fig. 10). Consequentially, the calmer water-surface would appear relatively darker in the SAR image [9], [12], [13], particularly when combined with the lower sensitivity of HH as compared to VV polarization to roughened water surfaces [13], [19]. These two contributing factors could have enhanced the discrimination between open water bodies and nonflooded marsh thereby contributing to the increased flood extent shown in early December. On the other hand, although offshore winds persisted in the first part of December, all site-specific recordings of water level gauges documented a water-level rise following 24 November that continued through the 13 December ASAR collection. In addition, fairly substantial rainfall events occurred on 25 November and 3 December, and were occurring around the time of the 13 December ASAR collection (Fig. 10). As in the sudden drop in inland water levels captured on the 24 November inundation recession, the 13 December ASAR change detection produced an expanded inundation complementing the water-levels pattern recorded by the inland hydrographs. In this case, the inundation distribution change seemed more traceable to prerainfall events than wind forcing.

VI. Conclusion

This study used a time series of Envisat ASAR scenes to demonstrate the utility of C-band SAR satellite data to map the history of storm-related flooding in a coastal wetland. Validated with inland hydrograph records, the co-occurrence of storm-surge flooding and its duration with marsh type produced information useful for determining the threshold of elevated salinity exposure and of saturation duration. These could be important parameters for assessing wetland status and predicting trends. In addition, the ability to relate an abrupt decrease of flooding to persistent offshore winds accompanying a storm front passage and a subsequent increase in nonsurge flooding to multiple rainfall events further demonstrated the potential of SAR to capture rapidly changing hydrologic events. The availability of this timely data source not only enhances the relevancy of inundation information to wetland status and trends, it alleviates many difficulties in using site-specific stage data to calibrate and validate hydraulic inundation models.

Similar to how a combination of SAR-derived flood extent and ancillary data sources, such as recorded water-levels and wind velocities, helped explain hydrodynamic events, LIDAR-based digital elevation model (DEM) data helped categorize flood recession patterns observed with SAR data. Even in this highly complex and dynamic coastal marsh landscape, drainage patterns were grouped into those associated with elevations < 80 cm and those ≥ 100 cm and a transition drainage pattern representing the 80 cm to < 100 cm elevations. Physically, marsh surface elevations < 80 cm were dominantly aligned with non-impounded marshes and elevations ≥ 100 cm with impounded marshes. Further, the coupling of the DEM and SAR-based flood extents showed that the abrupt drop in storm-surge flood extent was principally associated with impounded marshes. In both cases, the availability of timely flood extents and ancillary data sources provided direct information related to the hydraulic and hydrodynamic response of this coastal landscape.

In addition to advancing information related to changes in flood extent and distribution, polynomial trends relating incremental increases in the threshold value to positive change-detection outcomes exhibited correspondence to preceding storm surge and rainfall events. When these trends were parameterized for each pre- and post-ASAR change-detection date, the two indicator variables similarly indicated a relationship to preceding hydraulic conditions. If these inferred correspondences were verified and calibrated with ground-based measurements, the easily derived indicators could offer resource management a cost-effective and operational gauge of wetland hydraulic condition.

Even though we standardized the threshold for the like-polarized C-HH and C-VV SAR data and found good correspondence with hydrograph data and flood extent over time, we found threshold selection to be a laborious and time-consuming process. Proper selection required detailed examinations of incremental changes in the thresholds for each date and repetitive comparisons between flood extents created for separate dates. In addition, the threshold increments versus inundation trends indicated little ability to use automatic contouring to delineate the flood extents in these complex coastal marshes. Although the technique applied here for threshold selection was effective, more exploratory work is needed on the automated selection of thresholds used in the creation of SAR-based flood products of highly variable hydrologic environments.

Acknowledgment

Envisat ASAR data are copyrighted by the European Space Agency and were provided via Cat-1 2853 Project. The Landsat TM data are courtesy of the USGS EROS data center. Gratitude is extended to Dr. M. Kalcic and Dr. H. Wang for their thoughtful reviews and to L. Henry and B. Vairin of U.S. Geological Survey. The authors are very grateful for the incredible detail and insightful comments offered by the two anonymous reviewers. Mention of trade names does not constitute endorsement by the U.S. Government.

References

[1] R. Neyland, "The effects of Hurricane Rita on the aquatic vascular flora in a large fresh-water marsh in Cameron Parish, Louisiana," *CASTANEA*, vol. 72, no. 1, pp. 1–7, 2007.

[2] L. Kiage, N. Walker, S. Balasubramanian, A. Babin, and J. Barras, "Applications of Radarsat-1 synthetic aperture radar imagery to assess hurricane-related flooding of coastal Louisiana," *Int. J. Remote Sens.*, vol. 26, no. 24, pp. 5359–5380, 2005.

[3] E. Ramsey, III, D. Werle, Z. Lu, A. Rangoonwala, and Y. Suzuoki, "A case of timely satellite image acquisitions in support of coastal emergency environmental response management," *J. Coastal Res.*, vol. 25, no. 5, pp. 1168–1172, 2009.

[4] Y. Wang, "Seasonal change in the extent of inundation on floodplains detected by JERS-1 Synthetic Aperture Radar data," *Int. J. Remote Sens.*, vol. 25, no. 13, pp. 2497–2508, 2004.

[5] M. Lang, P. Townsend, and E. Kasischke, "Influence of incidence angle on detectiing flooded florests using C-HH synthetic aperture radar data," *Remote Sens. Environ.*, vol. 112, pp. 3898–3907, 2008.

[6] J. Töyra and A. Pietroniro, "Towards operational monitoring of a northern wetland using geomatics-based techniques," *Remote Sens. Environ.*, vol. 97, pp. 174–191, 2005.

[7] L. Hess, J. Melack, S. Filoso, and Y. Wang, "Delineation of inundated area and vegetation along the Amazon Floodplain with the SIR-C synthetic aperture radar," *IEEE Trans. Geosci. Remote Sens.*, vol. 33, no. 4, pp. 896–904, 1995.

[8] E. Ramsey, III, "Monitoring flooding in coastal wetlands by using radar imagery and ground-based measurements," *Int. J. Remote Sens.*, vol. 16, pp. 2495–2502, 1995.

[9] D. Werle, T. Martin, and K. Hasan, "Flood and coastal zone monitoring in Bangladesh with Radarsat ScanSAR: Technical experience and institutional challenges," *Johns Hopkins APL. Tech. Dig.*, vol. 21, no. 1, pp. 148–154, 2000.

[10] V. Klemas, J. Dobson, R. Ferguson, and K. Haddad, "A coastal land cover classification system for the NOAA Coastwatch Change analysis project," *J. Coastal Res.*, vol. 9, no. 3, pp. 862–872, 1993.

[11] R. Lunetta, J. Lyon, B. Guindon, and C. Elvidge, "North American landscape characterization dataset development and data fusion issues," *Photogramm. Eng. Remote Sens.*, vol. 64, no. 8, pp. 821–829, 1998.

[12] L. Smith, "Satellite remote sensing of river inundation area, stage, and discharge: A review," *Hydrol. Processes*, vol. 11, pp. 1427–1439, 1997.

[13] J. Henry, P. Chastanet, K. Fellah, and Y. Desnos, "Envisat multi-polarized ASAR data for flood mapping," *Int. J. Remote Sens.*, vol. 27, no. 10, pp. 1921–1929, 2006.

[14] E. Ramsey, III, "Radar remote sensing of wetlands," in *Remote Sensing Change Detection: Environmental Monitoring Methods and Applications*, R. Lunetta and C. Elvidge, Eds. Ann Arbor, MI: Ann Arbor Press, 1998, pp. 211–243.

[15] E. Ramsey, III, "Remote sensing of coastal environments in Encyclopedia of Coastal Science," in *Encyclopedia of Earth Sciences Series*, M. L. Schwartz, Ed. Dordrecht, The Netherlands: Kluwer Academic Publishers, 2005, pp. 797–803.

[16] J. Ormsby, B. Blanchard, and A. Blanchard, "Detection of lowland flooding using active microwave systems," *Photogramm. Eng. Remote Sens.*, vol. 51, pp. 317–328, 1985.

[17] M. Moghaddam, K. McDonald, J. Cihlar, and W. Chen, "Mapping wetlands of North American boreal zone from satellite radar imagery," in *Proc. Geosci. Remote Sens. Symp., IGARSSS '03*, Toulouse, France, 2003, pp. 261–263.

[18] R. Leconte and T. Pultz, "Evaluation of the potential of Radarsat for flood mapping using simulated satellite SAR imagery," *Canadian J. Remote Sens.*, vol. 17, pp. 241–249, 1991.

[19] P. Matgen, G. Schumann, J. Henry, L. Hoffmann, and L. Pfister, "Integration of SAR-derived river inundation areas, high-precision topographic data and a river flow model toward near real-time flood management," *Int. J. Appl. Earth Obs. Geoinf.*, vol. 9, pp. 247–263, 2007.

[20] E. Kasischke, K. Smith, L. Bourgeau-Chavez, E. Romanowicz, S. Brunzell, and C. Richardon, "Effects of seasonal hydrologic patterns in south Florida wetlands on radar backscatter measured from ERS-2 SAR imagery," *Remote Sens. Environ.*, vol. 88, pp. 423–441, 2003.

[21] E. Ramsey, III, Z. Lu, A. Rangoonwala, and R. Rykhus, "Multiple baseline radar interferometry applied to coastal landcover classification and change analyses," *GIScience Remote Sens.*, vol. 43, no. 4, pp. 283–309, 2006.

[22] Z. Lu and O. Kwoun, "Radarsat-1 and ERS InSAR analysis over southeastern coastal Louisiana: Implication for mapping water-level changes beneath swamp forests," *IEEE Trans. Geosci. Remote Sens.*, vol. 46, no. 4, pp. 2167–2184, 2008.

[23] A. Lewis, F. Henderson, and D. Holcomb, "Radar fundamentals: The geoscience perspective," in *Principles and Applications of Imaging Radar*, F. Henderson and A. Lewis, Eds. New York: Wiley, 1998, pp. 131–181.

[24] The Earth Observation Handbook, Climate Change Special Edition, CEOS, Committee on Earth Observation Satellite, 2008 [Online]. Available: http://www.eohandbook.com

[25] K. Pope, E. Rejmankova, J. Paris, and R. Woodruff, "Detecting seasonal flooding cycles in marshes of the Yucatan Peninsula with SIR-C polarimetric radar imagery," *Remote Sens. Environ.*, vol. 59, pp. 157–166, 1997.

[26] F. Grings, P. Ferrazzoli, H. Karszenbaum, J. Tiffenberg, P. Kandus, L. Guerriero, and J. Jacobo-Berrles, "Modeling temporal evolution of Junco marshes radar signatures," *IEEE Trans. Geosci. Remote Sens.*, vol. 43, no. 10, pp. 2238–2245, 2005.

[27] M. Dobson, L. Pierce, and F. Ulaby, "Knowledge-based land-cover classification using ERS-1/JERS-1 SAR composites," *IEEE Trans. Geosci. Remote Sens.*, vol. 34, no. 1, pp. 83–99, 1996.

[28] S. Hong, S. Wdowinski, and S. Kim, "Evaluation of TerraSAR-X observations for wetland InSAR application," *IEEE Trans. Geosci. Remote Sens.*, vol. 48, no. 2, pp. 864–873, 2010.

[29] R. Knabb, D. Brown, and J. Rhome, Tropical Cyclone Report Hurricane Rita 18–26 September 2005, National Hurricane Center, 2006 [Online]. Available: http://www.timothyhorrigan.com/documents/hurricane/TCR-AL182005_Rita.pdf

[30] C. Nielsen and D. Werle, "Do long-term space plans meet the needs of the mission to Planet Earth?," *Space Policy*, vol. 9, no. 1, pp. 11–16, Feb. 1993.

[31] R. Chabreck, "Marsh Zones and Vegetative Types in the Louisiana Coastal Marshes," Ph.D. dissertation, Louisiana State Univ., Baton Rouge, LA, 1970.

[32] R. Morton, J. Bernier, J. Barras, and N. Ferina, "Rapid Subsidence and Historical Wetland Loss in the Mississippi Delta Plain: Likely Causes and Future Implications," USGS, Open-File Report 2005-1216, 2005.

[33] Envisat ASAR Product Handbook, no. 2.2, European Space Agency (ESA), Feb. 2007 [Online]. Available: http://envisat.esa.int/handbooks/asar/

[34] Strategic Online Natural Resources Information System, SONRIS Integrated Applications, Louisiana Dept. Natural Resources, Jul. 8, 2009 [Online]. Available: http://sonris-www.dnr.state.la.us/www_root/sonris_portal_1.htm

[35] Louisiana GIS Digital Map of May 2007, Louisiana Oil Spill Coordinator's Office (LOSCO), 2007.

[36] C. Sasser, J. Visser, E. Mouton, J. Linscombe, and S. Hartley, "Vegetation Types in Coastal Louisiana in 2007," U.S. Geological Survey, Open-File Report 2008-1224, 2008.

[37] Atlas: The Louisiana Statewide GIS LSU CADGIS Research Lab., Baton Rouge, LA [Online]. Available: http://atlas.lsu.edu

[38] Observational Data Interactive Navigation, NOAA Tides and Currents Center for Operational Oceanographic Products and Services. National Ocean Service, National Oceanic and Atmospheric Administration, Sep. 13, 2009 [Online]. Available: http://tidesandcurrents.noaa.gov/gmap3/

[39] NOAA Satellite and Information Service. National Ocean Service, National Oceanic and Atmospheric Administration, National Climate Date Center, Oct. 14, 2009 [Online]. Available: http://lwf.ncdc.noaa.gov/oa/ncdc.html

[40] E. Ramsey, III, S. Laine, D. Werle, B. Tittley, and D. Lapp, "Monitoring Hurricane Andrew damage and recovery of the coastal Louisiana marsh using satellite remote sensing data," in *Proc. Coastal Zone Canada '94*, 1994, pp. 1841–1852.

[41] E. Ramsey, III, G. Nelson, F. Baarnes, and R. Spell, "Light attenuation profiling as an indicator of structural changes in coastal marshes," in *Remote Sensing and GIS Accuracy Assessment*, R. Lunetta and J. Lyon, Eds. New York: CRC Press, 2004, pp. 59–73.

[42] C. Elachi, *Spaceborne Radar Remote Sensing: Applications and Techniques*. New York: IEEE Press, 1988.

[43] E. Ramsey, III, G. Nelson, S. Sapkota, S. Laine, J. Verdi, and S. Krasznay, "Using multiple polarization L band radar to monitor marsh burn recovery," *IEEE Trans. Geosci. Remote Sens.*, vol. 37, no. 1, pp. 635–639, 1999.

[44] A. Chanzy, "Basic soil surface characteristics derived from active microwave remote sensing," *Remote Sens. Rev.*, vol. 7, no. 3, pp. 303–319, 1993.

[45] L. Narcisse, Lacassine National Wildlife Refuge, Comprehensive Conservation Plan. U.S. DoI, Fish & Wildlife Service, 2007 [Online]. Available: http://www.fws.gov/swlarefugecomplex/pdf/Lac09%20huntEA.pdf

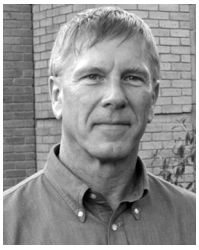

Elijah Ramsey III is a principal investigator of terrestrial and coastal ocean remote sensing and image processing in the U. S. Geological Survey, National Wetlands Research Center, Lafayette, LA. He received the B.S. in chemistry from the University of Oregon, the M.S. in geophysical sciences from the Georgia Institute of Technology, Atlanta, Georgia, and the Ph.D. from the Department of Geography at the University of South Carolina. His applied research is focused on producing consistent biophysical information directly relevant to sustaining critical natural resources that support the well-being of human and wildlife populations. As part of this focus, his work integrates data from passive to active and optical to radar systems that advance the response and strategic monitoring of natural resources and the human populations and facilities that occupy these environments.

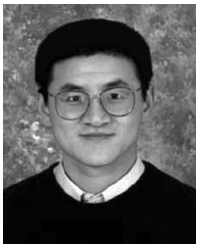

Zhong Lu received the M.S. degree from Beijing University, China, in 1992 and the Ph.D. from the University of Alaska Fairbanks in 1996.

He is a physical scientist with Cascades Volcano Observatory, U.S. Geological Survey (USGS). He is a principal investigator of projects funded by the NASA, European Space Agency, Japan Aerospace Exploration Agency, German Space Agency and USGS on the study of land surface deformation using satellite InSAR imagery. His research interests include technique developments of SAR, InSAR and persistent scatterer InSAR processing, and their applications on natural hazards monitoring and natural resources management. He was the recipient of the 2001 Raytheon Distinguished Level Award for Excellence in Technology, and the 1999 Jerald J. Cook Memorial Award. He has been a committee member of the International User Team for Radarsat-C SAR Constellations, the GeoEarthscope InSAR User Working Group, and the NASA's Alaska Satellite Facility User Working Group, and serves on editorial boards of three international journals.

Yukihiro Suzuoki received the B.S. and M.S. degree in civil engineering from Nihon University, Chiba, Japan, in 1998 and 2000, respectively, and the M.A. degree in geography from Kent State University, Ohio, in 2008.

He is currently working as a Remote Sensing Specialist II, for ASci Inc., at the U.S. Geological Survey, National Wetlands Research Center, Lafayette, LA. His research interests include monitoring and detecting environmental changes in the coastal wetlands using both optical and radar sensors.

Amina Rangoonwala received the M.Sc. degree in physics from the University of Karachi, Pakistan, in 1984. In 2000 she immigrated to the United States. She has since been working at the USGS National Wetlands Research Center, Lafayette, LA, as a remote sensing specialist for IAP World Services Inc. She is working on projects applying hyperspectral image analysis to determine the onset and progression of vegetation decline, detection of the invasive species occurrences, and leaf optics measurements for ground base validation. Her work also involves the integration of optical and radar satellite data to support emergency response activities, for monitoring and mapping flood waters along the US gulf coast, and polarimetric radar for detecting sub-canopy toxic spill presence and change in canopy structure.

Dirk Werle (M'88) received the M.Sc. in physical geography and remote sensing from McGill University, Canada, in 1984, after undergraduate studies at Trier University in Germany. He is a geoscientist and partner with ÆRDE Environmental Research in Halifax, Nova Scotia, Canada. He has worked as a consultant and advisor for several Canadian government agencies, including the Canada Centre for Remote Sensing and the Canadian Space Agency over the past 20+ years, notably in the field of satellite SAR applications. In the late 1980s he authored under contract to CCRS the 1st and 2nd edition of "Radar Remote Sensing—A Training Manual" for use in Canadian universities and at international teaching institutions. He taught Remote Sensing as a sessional lecturer at Carleton University in Ottawa, Canada, and Saint Mary's University in Halifax for several years. He is an associate fellow and member of the executive of the Canadian Remote Sensing Society and also served as its Chairman from 2003–2005. He has been a member of IEEE GRSS since 1988 and currently serves as a vice-chair of the Canadian Atlantic Section in IEEE Region 7.